Towards a Consistent Conventional Treatment of Surface-Load Induced Deformations

Hans-Peter Plag* Geoff Blewitt Thomas A. Herring

Abstract

To be added.

1 Introduction

At time scales from sub-daily to decades, the largest mass redistributions on the surface of the solid Earth mainly occur in the global hydrological cycle, i.e., the water stored in atmosphere, ocean, on land, in glaciers, and ice sheets. Exchanges of mass between these major reservoirs of the hydrological cycle are linked to each other through a conservation-of-mass equation (Clarke et al., 2005). The mass movements load and deform the solid Earth. With respect to the signal in geodetic parameters we note that any of these mass movements changes the Earth's gravitational field primarily due to the mass redistribution, and, secondarily, due to deformations of the solid Earth. Through associated changes in the angular momentum and the moments of inertia of atmosphere, ocean, terrestrial hydrosphere, and solid Earth the redistribution of mass in the fluid envelope also affects the rotation of the Earth. Moreover, variation in the first-degree spherical harmonic component of surface mass (caused by inter-hemispheric mass exchange) displaces the *Center of Mass of the solid Earth* (CE) with respect to the ITRF origin, which is the *Center of Mass of the whole Earth system* (CM, Blewitt et al., 2001; Lavallee & Blewitt, 2002; Blewitt, 2003; Lavallée et al., 2006). Any of these changes will affect the mass distribution in the ocean and thus create additional loads and variations in the geodetic parameters. Therefore, the geodetic loading signals of atmosphere, ocean, and terrestrial hydrosphere are inherently linked together (Blewitt & Clarke, 2003) and an integrated gravitationally consistent modeling approach is required in order to predict these geodetic signals with high accuracy.

Statement 1 (S1): *The geodetic signals of mass redistribution in the global hydrological cycle need to be modeled in a gravitationally consistent integrated model of the Earth system accounting for the linkage between reservoirs in the hydrological cycle as well as the feedback of the changes in Earth's shape, gravity field and rotation on the distribution of mass in these reservoirs.*

In the IERS Conventions (McCarthy & Petit, 2004), the geodetic signals of mass redistribution in the hydrological cycle are currently not covered by conventional models. However, these signals are well above the anticipated accuracy goal of 10^{-9} or better. Therefore, the question arises whether and how these signals can be addressed through appropriate conventions.

The current approach to the conventional global *International Terrestrial Reference Frame* (ITRF) is based on a global polyhedron of a low number of points (approximately 500) with the trajectories of these points given by a linear functional model describing the secular point motion (the *regularized coordinates*, McCarthy & Petit, 2004), which is augmented by a small number of models accounting for high-frequency motion caused by a set of individual geophysical processes. Thus, the secular part of the polyhedron is basically determined by a set of coordinates $\vec{X}_0^{(i)},\ i = 1, ..., N$ and velocities $\vec{V}_0^{(i)},\ i = 1, ..., N$, with N being the number of vertices of the polyhedron. The

*Nevada Bureau of Mines and Geology, UNR, Reno, Nevada; e-mail: hpplag@unr.edu

trajectories of the vertices of the secular polyhedron are given by

$$\vec{X}^{(i)}(t) = \vec{X}_0^{(i)} + \vec{V}_0^{(i)}(t - t_0),\ i = 1, ..., N, \tag{1}$$

where t_0 is the reference epoch. Once determined, the polyhedron realizes implicitly the axes, origin and scale of an underlying Cartesian coordinate system rotating with the solid Earth. The coordinates and velocities of the corner points are determined from observations such that they are consistent with a set of conventional constants and constraints.

For space-geodetic analysis, the station motion model needs to account for short-period fluctuations. Depending on the length of the analysis interval, the station motion model may be represented as

$$\vec{X}(t) = \vec{X}(t_c) + \sum_{k=1}^{K} \vec{g}_k(t) \tag{2}$$

(for short observation intervals, e.g. 1 day), where t_c is the center epoch of the observation interval, or

$$\vec{X}(t) = \vec{X}(t_0) + \vec{V}_0(t - t_0) + \sum_{k=1}^{K} \vec{g}_k(t) \tag{3}$$

(for longer observation intervals, e.g. 1 year). Here, the $\vec{g}_k(t)$ are predictions of the point displacements based on *a priori* models of geophysical processes. Since the secular reference polyhedron depends on the station motion model used in the space-geodetic analyses, these models have to be conventional models.

Currently, the IERS Conventions with respect to the reference point displacements (McCarthy & Petit, 2004, Chapter 7,) cover geophysical contributions of Earth's rotation changes ("pole tide"), solid Earth tides, and ocean tidal loading. Most likely atmospheric tidal loading will be added soon. Concerning atmospheric loading, it is stated that global geophysical models should be used, although it is recognized that these models have a number of problems. A local approach based on regression coefficients is rejected for various reasons. Non-tidal ocean loading and loading of the terrestrial hydrosphere are not addressed to any level of detail.

Increased accuracy requirements have stimulated a discussion of whether and how to include the loading signal due to (non-tidal) atmospheric, (terrestrial) hydrological, and non-tidal ocean loading in the conventional station motion model (see e.g., Van Dam et al., 2003, for a discussion). The standard way of thinking is along the line of adding *a priori* models for each of the geophysical processes to the IERS Conventions. Ray et al. (2007) propose principles to be follow in the selection of models to be included. Although these principles establish clear rules and model priorities, it must be questioned whether this approach will be sufficient to satisfy current and future accuracy and other user requirements. In particular, increasing successively the set of separate conventional models for potentially correlated phenomena does not appear to be suitable below a certain accuracy level. Considering the accuracy goal of the *Global Geodetic Observing System* (GGOS) of 10^{-9} or better, the interactions between different processes may be well above this accuracy level but not be captured by the current approach. Moreover, consistency of changes in Earth's shape, gravity field and rotation may also require a more integrated approach to the station motion model that accounts for the interaction of processes and the common effects of these processes on shape, gravity field and rotation.

Statement 2 (S2): *A conventional approach to load-induced geodetic signals based on separate models for the main reservoirs of the global hydrological cycle will not meet the accuracy and consistency goal of* 10^{-9}.

In order to explore steps towards a consistent treatment of surface loading effects on Earth's shape, gravity field, and rotation in agreement with Statement 1, we will first consider the main applications of terrestrial reference frames with the goal to establish general requirements for the frame and the access to it (Section 2). By comparing the current frame to these requirements, a critique of the current approach will emerge pointing in the direction to go (Section 3). This will lead us to a proposal for a different and more integrated approach to the future terrestrial

reference frame (Section 4) replacing the current polyhedron and set of single-process models by an integrated *Dynamic Reference Earth Model* (DREM) (as originally proposed by Herring et al., 2007). Achieving a more consistent treatment of surface-load signals poses a number of theoretical and practical problems, of which we address a few examples (Section 6). Although it is clear that for some time to come the current approach will persist, we argue that in order to achieve the goals of GGOS, progress towards a more integrated approach is essential. Therefore, any extensions of the Conventions aiming at the inclusion of conventional models for surface loading should be compliant with the goal of consistency as described above, and we discuss some immediate improvements (Section 7), before we summarize a set of recommendations (Section 8).

2 Setting the stage

A terrestrial reference frame has little value by itself. It is through the applications that a reference frame gains importance and value. Therefore, any discussion about a reference frame and its potential improvements needs to be based on a clear understanding of the applications of this particular reference frame. Therefore, we have to ask what our goals and applications are for a modern global geodetic reference frame.

In the past, a main goal of a reference frame, no matter whether it was local, national, or regional, was to allow for the determination of positions with respect to this frame. An underlying more or less static view led to a concept of time-independent coordinates. Reference frames were realized through networks of points with fixed coordinates, and positions were determined relative to nearby reference points.

The development of space-geodetic techniques and the continuous improvement of measurement accuracy has enabled us to observe extremely small point motion (displacements) in a global reference frame. For many scientific and societal applications, time series of point displacements with respect to the reference frame have become a key goal. Being able to observe time series of point displacements has obvious and many benefits, for example, in Earth sciences, global change monitoring, geohazards assessment, disaster mitigation, and monitoring of infrastructure. The most demanding scientific and non-scientific requirements concerning positioning and terrestrial geodetic reference frames do not only demand increasing accuracy and temporal stability, but also high spatial and temporal resolution and low latency (Gross et al., 2007a). In order to meet these demands, it is increasingly important to be able to predict reference trajectories for all points on the Earth surface, against which "anomalous motion" can be detected. To meet these requirements, a reference frame is needed that allows the prediction of point motion with high spatial and temporal resolution.

Statement 3 (S3): *Condensing the essential goal of a global terrestrial reference frame, we state that while the primary goal in the past was to allow for the determination of point position, the primary goal today is to allow for the monitoring of point motion.*

Many application require high accuracy and stability in order to detect small "anomalous displacements". For most of these applications, a reference frame today has to be established locally, among others, posing the problem of identifying a stable local reference. However, the most rational approach in terms of required local expertise and infrastructure would be a global frame accessible anywhere on Earth. The goal of such a frame would be to minimize point displacements with respect to the frame, so that most observed displacements would be due to unaccounted processes. In order to achieve this goal, the predictive capabilities of the reference frame need to be improved as much as possible. The ideal situation would be that the motion of all points could be predicted with very high accuracy.

Attempts to establish reference frames that minimize point displacements have been rather successful on regional level. Thus, the regional frames EUREF (e.g. Altamimi & Boucher, 2002) and SNARF (Blewitt et al., 2004) reduce the residual secular horizontal displacements of most points to a few mm/yr, particularly if more advanced geophysical models are included in the frame definition (see, e.g., Plag et al., 2002). However, on global scales, the ITRF results in residual secular point motions much larger than that. Moreover, large intraseasonal to interannual displacements are present in particular in the time series of vertical displacements (order ± 20 mm).

3 The order of the problem

The simple mathematical model of regularized coordinates has three major problems: (1) The actual motion of the reference points is not linear in general. Deviations from linear motion are due to tides, surface loading, and processes in the solid Earth, including pre-, co-, and postseismic displacements. For large earthquakes, the latter can be of regional to global nature. Currently, only non-linear displacements due to tides are taken into account. (2) The methodology used for the alignment of solutions to the ITRF as well as the conventional mathematical model for the reference point motion constitute a technique- and solution-dependent filtering of unmodeled geophysical signals, which aliases these signals into displacement time series and hampers comparison of observations to model predictions and between techniques. (3) The velocity vectors have errors, which over time can deform the polyhedron considerably, thus requiring frequent updates of ITRF.

In order to be able to assign predicted (expected) reference motion to any point on the Earth's surface, knowledge of the global velocity field $\vec{V_0} = f(\vec{X})$ would be required. This is currently not available. However, with the help of precise satellite orbits and clocks, precise point coordinates can be determined for any point in ITRF. Precise orbits and clocks are determined on a daily basis in a free solution which is then aligned to the reference frame. The methodology used for this alignment as well as the mathematical model for the reference point motion determines the degree to which geophysical signals are filtered and potentially aliased into the displacement time series.

In Figure 1, time series of vertical displacements for selected North American stations are shown. Day-to-day variation and intraseasonal to interannual variations are of the order of ± 20 mm and ± 10 mm, respectively. Most station exhibit a linear trend, and a seasonal cycle is discernible. For stations separated on the order of 10^3 km, considerable differences in the intraseasonal and interannual variations are visible (Figure 1, upper diagrams). On local scale (up to 500 km), the differences on intra- to interannual time scales are very small, while the main difference are in the day-to-day variations (Figure 1, lower diagrams for the Basin and Range Province).

The displacement time series are a combination of geophysical signals and apparent displacements induced by the GPS system and data analysis. Concerning the observed interannual variations, a key problem is the separation of instrumental and analysis effects from the geophysical signals. The interannual variations have surprisingly small spatial scales, of the order of 10^3 km, with significant spatial variations over North America. If these variations were solely due to GPS-system and analysis effects, we would expect larger spatial scales in these variations.

From Figure 1 it is obvious that both linear and non-linear motions deduced from these time series depend strongly on the time interval chosen. Using various filter techniques (e.g., Wdowinski et al., 1997, 2004), the so-called *Common Mode Variations* (CMVs) can be reduced. However, the result depends on the time interval and spatial extent of the network considered. Consequently, geophysical interpretation of the resulting displacement time series is hampered by the dependence on the applied filters and a general non-uniqueness of the time series.

Cross-correlation between stations is also strongly affected by the space-geodetic analysis, the strategy used for the alignment to ITRF, and the (implicit) spatial and temporal filtering. As an example, in Figure 2, we show the cross-correlation for a set of European stations, for which several displacement time series were determined from the same observations using different analysis strategies (for details on the analyses, see Kierulf et al., 2007). The large variations in the spatial pattern of cross correlation for the different analyses underlines the potential bias of displacement time series with respect to geophysical processes not accounted for in the reference frame alignment or the station motion model.

One consequence of the dependence of displacement time series on the analysis and reference frame alignment strategy is that a straight-forward comparison of predicted and observed observations is not justified. This seriously hampers model validation. For example, in a study of displacement time series determined from GPS observations, Dong et al. (2002) found that the predicted seasonal signal due to loading caused by atmosphere and hydrosphere did not match the observed seasonal signal and concluded that other processes must be contributing to the observed signal. A comparison of the predictions of atmospheric loading to GPS-displacement time series also shows that the observations only capture about 70% of the predicted signal (Table 1). This general reduction of the geophysical loading signal may be the result of (1) errors in the predictions, (2) reduction of the signal in the observations due to implicit spatial filtering,(3) anti-correlated geophysical processes leading to a partial cancellation of the loading signal, (4) the effect of systematic errors in separating the effects of wet and hydrostatic atmospheric delays (e.g.,

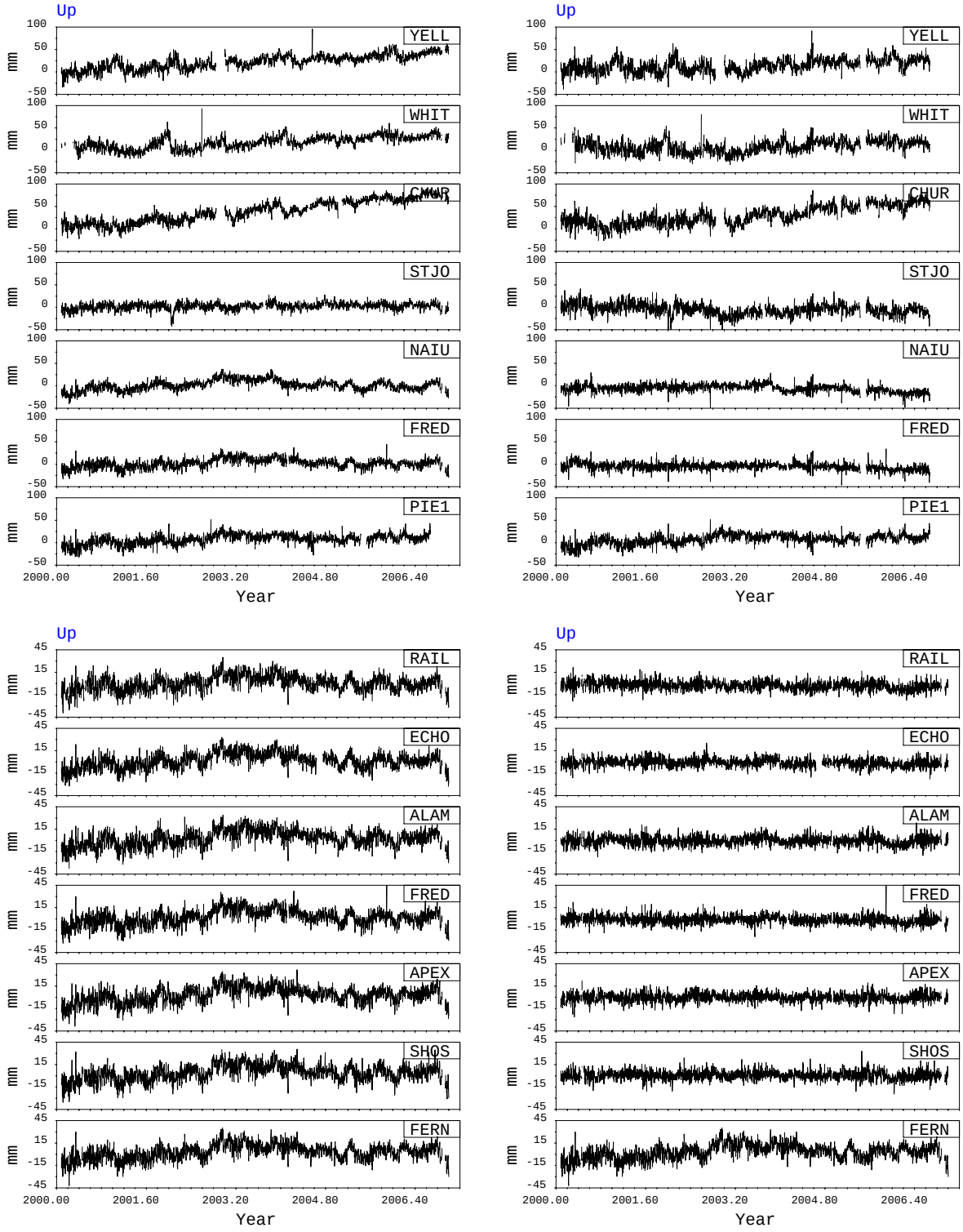

Figure 1. Time series of vertical displacements. Upper two blocks of diagrams: Selected North American stations distributed from 31°to 65°N. Lower two blocks of diagrams: Stations in the Basin and Range Province. In each pair of diagrams, the time series of vertical displacements are shown in the left diagram, while the right diagram shows for each station the difference to the time series shown at the bottom of the right diagrams. The offset around Nov. 5, 2006 is due to the transition from JPL00 (based on ITRF2000) to IGS05 (based on ITRF2005).

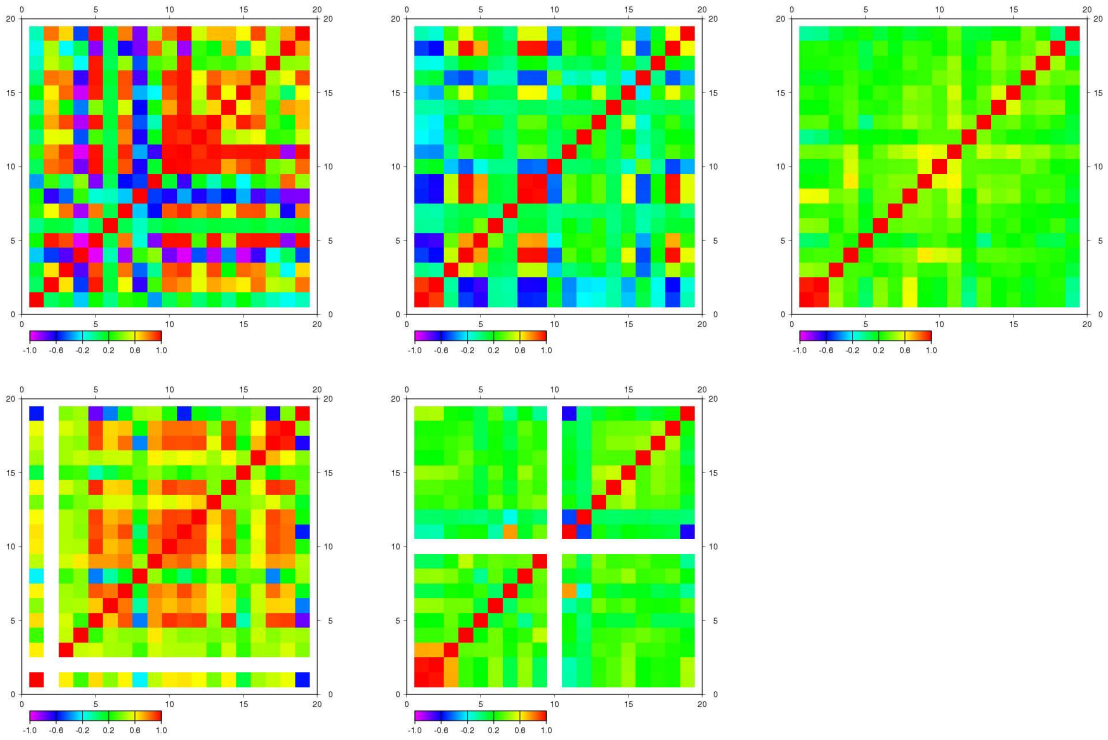

Figure 2. Interstation correlation for different analysis strategies. Each diagram shows for the same set of 19 European stations the crosscorrelation coefficient of pairs of time series of the vertical displacement computed with different analysis strategies. Stations are roughly sorted according to latitude (with the latitude ranging from 79.93°N (NYAL) to 35.50°N (LAMP). White bands indicate that a particular station was not included in an analysis. Analyses are (from upper left diagram to lower right diagram: 1: GIPSY with IGS orbits and clocks, 2: Bernese in PPP mode, 3: GAMIT, 4: Bernese in double-difference mode, 5: GIPSY with JPL orbits and clocks. For details see Kierulf et al. (2007). Stations are: 1: nya1 (78.92956°N, 11.86531°E), 2: nyal (78.92958°N, 11.86508°E), 3: ando (69.27837°N, 16.00870°E), 4: helg (54.17448°N, 7.89309°E), 5: wlad (54.79676°N, 18.41875°E), 6: morp (55.21279°N, 358.31451°E), 7: nstg (55.00742°N, 358.56012°E), 8: live (53.44970°N, 356.98178°E), 9: lowe (52.47322°N, 1.75020°E), 10: shee (51.44568°N, 0.74341°E), 11: pmtg (50.80233°N, 358.88879°E), 12: camb (50.21844°N, 354.67264°E), 13: newl (50.10303°N, 354.45721°E), 14: alac (38.33892°N, 359.51877°E), 15: lago (37.09894°N, 351.33163°E), 16: geno (44.41939°N, 8.92114°E), 17: cagl (39.13591°N, 8.97275°E), 18: lamp (35.49977°N, 12.60566°E), 19: vene (45.43698°N, 12.33198°E).

Table 1. Station dependent regression and correlation coefficients for observed and predicted vertical land motion. Stations are European CGPS sites (mainly stations of the IGS network or the EPN). The loading predictions are as given in Table 2. The regression and correlation coefficients are computed for pairs of time series of vertical land motion observed by CGPS and one of the five different loading predictions. Time interval is 2000.0 to 2004.0. The regression coefficients are dimensionless.

No.	Station	P1	P2	P3	P4	P5
		Regression coefficients				
1	BOR1	0.861	0.676	0.943	0.731	0.821
2	BRUS	0.754	0.290	0.842	0.642	0.675
3	BUCU	1.166	0.864	1.191	0.879	1.094
4	BZRG	0.970	0.708	0.879	0.627	0.803
5	CAGL	0.326	0.292	0.538	0.453	0.263
6	EBRE	0.828	0.583	0.795	0.604	0.648
7	GENO	0.627	0.426	0.695	0.492	0.539
8	GOPE	0.817	0.656	0.855	0.705	0.752
9	GRAS	0.424	0.267	0.537	0.341	0.464
10	GRAZ	0.806	0.651	0.826	0.673	0.723
11	HERS	0.644	0.504	0.779	0.619	0.558
12	HFLK	0.630	0.350	0.733	0.438	0.615
13	JOZE	0.928	0.682	0.955	0.707	0.820
14	KOSG	0.799	0.618	0.878	0.678	0.701
15	LAMA	0.675	0.550	0.721	0.587	0.671
16	MATE	0.541	0.381	0.844	0.492	0.728
17	MEDI	0.517	0.345	0.593	0.432	0.530
18	METS	0.579	0.478	0.674	0.525	0.531
19	ONSA	0.607	0.469	0.791	0.548	0.568
20	POTS	0.844	0.672	0.952	0.739	0.825
21	SFER	0.753	0.493	0.672	0.484	0.606
22	SOFI	0.941	0.707	0.922	0.686	0.894
23	TROM	0.816	0.547	0.940	0.596	0.683
24	VENE	0.794	0.718	0.714	0.684	0.679
25	VILL	0.496	0.332	0.494	0.362	0.446
26	WSRT	0.749	0.541	0.890	0.628	0.674
27	WTZT	0.800	0.623	0.845	0.663	0.718
28	ZIMM	0.553	0.393	0.581	0.442	0.570
	MEAN	0.723	0.529	0.788	0.588	0.664

No.	Station	P1	P2	P3	P4	P5
		Correlation coefficients				
1	BOR1	0.464	0.423	0.468	0.420	0.424
2	BRUS	0.356	0.178	0.363	0.309	0.337
3	BUCU	0.464	0.430	0.438	0.400	0.402
4	BZRG	0.340	0.291	0.294	0.243	0.277
5	CAGL	0.071	0.087	0.069	0.094	0.066
6	EBRE	0.227	0.196	0.221	0.198	0.184
7	GENO	0.215	0.179	0.210	0.181	0.192
8	GOPE	0.358	0.337	0.362	0.343	0.328
9	GRAS	0.135	0.105	0.135	0.109	0.137
10	GRAZ	0.334	0.320	0.327	0.310	0.294
11	HERS	0.260	0.228	0.263	0.236	0.254
12	HFLK	0.266	0.174	0.291	0.202	0.263
13	JOZE	0.389	0.336	0.391	0.334	0.339
14	KOSG	0.415	0.364	0.426	0.369	0.387
15	LAMA	0.325	0.309	0.326	0.308	0.315
16	MATE	0.159	0.149	0.167	0.143	0.179
17	MEDI	0.190	0.156	0.208	0.181	0.196
18	METS	0.383	0.362	0.378	0.343	0.357
19	ONSA	0.367	0.325	0.361	0.297	0.350
20	POTS	0.450	0.412	0.449	0.401	0.417
21	SFER	0.199	0.171	0.189	0.170	0.174
22	SOFI	0.270	0.263	0.248	0.235	0.250
23	TROM	0.369	0.289	0.368	0.276	0.332
24	VENE	0.214	0.234	0.191	0.214	0.184
25	VILL	0.143	0.110	0.149	0.123	0.129
26	WSRT	0.416	0.343	0.432	0.348	0.402
27	WTZT	0.340	0.309	0.335	0.304	0.306
28	ZIMM	0.241	0.200	0.251	0.218	0.249
	MEAN	0.299	0.260	0.297	0.261	0.276

the use of a constant surface pressure to model the atmospheric delays Tregoning & Herring, 2006). While (1) and (3) cannot be excluded, we anticipate that a combination of (2) and (4) is the main cause for the mismatch between predictions and observations. The effect bof (4) could be mitigated through improved analysis, while the mitigation of (2) requires a different approach to the alignment of the solutions to the global reference frame.

Statement 4 (S4): *Space-geodetic time series of Earth's surface point displacements contain non-geophysical signals and sub-daily to decadal geophysical signals are significantly biased.*

4 Extending the reference frame concept

It would be of great advantage if more elaborate models were available that could predict the Earth's surface motion with high accuracy at time scales from sub-daily to secular. In this case, a DREM could be agreed upon, and the secular model defined by eq. (1) could be replaced by

$$\vec{X}(t) = \vec{X}_0 + \delta\vec{X}(t), \tag{4}$$

Table 2. Models and input data set used for predictions of displacements induced by atmospheric loading. The predictions are denoted as P1 to P5. Sources for air pressure fields are European Center for Medium Range Weather Forecast (ECMWF) and National Center for Environmental Prediction (NCEP). Origin of the reference frames are the Center of mass of the solid Earth (CE) and the Center of Mass of the earth system (CM), which in this case means the solid Earth and the atmosphere. Earth models are PREM (Dziewonski & Anderson, 1981) and G+B (Gutenberg - Bullen, see Farrell, 1972). Computation methods are SHE: Summation of spherical Harmonic Expansion, and CGF: Convolution of Green's Function and load anomaly. Authors are PG: Pascal Gegout, TvD: Tonie van Dam. Data source is http://www.sbl.statkart.no.

Prediction	Input	Ref.Fr.	Earth M.	Comp.	Author
P1	ECMWF	CE	PREM	SHE	PG
P2	ECMWF	CM	PREM	SHE	PG
P3	NCEP	CE	PREM	SHE	PG
P4	NCEP	CM	PREM	SHE	PG
P5	NCEP	CE	G+B	CGF	TvD

where the displacement field $\delta\vec{X}(t)$ is predicted by the DREM. In principle, the DREM could predict the displacement field $\delta\vec{X}(t)$ for any point on the Earth's surface and for any time t. "Anomalous motion" could be defined as deviation from the motion predicted by the DREM. This rigorous approach is sketched by Herring et al. (2007). It is the anomalous motion, which is of interested both scientifically and for practical purposes such as monitoring potentially hazardous (i.e., seismic, volcanic, instable) areas.

In order to achieve a physically meaningful terrestrial reference frame, the DREM has to account for most of the known geophysical signals. In the absence of a sufficiently elaborated integrated Earth system model, a step towards a DREM could be a set of independent nested models, with each of them representing a subset of the relevant physical processes, including coseismic and postseismic displacements of great earthquakes, atmospheric, hydrological, and cryospheric loading, ocean tidal and non-tidal loading, and postglacial rebound. For this composite model, the displacement field would be described by

$$\delta\vec{X}(\vec{X},t) = \sum_{j=1}^{M} \vec{g}_j(\vec{X},t), \tag{5}$$

where the $\vec{g}_j,\ j = 1, M$ are the displacement fields determined from the M geophysical models representing processes such as Earth tides, surface loading, earthquakes, and other surface displacements. In principle, this would be an easy-to-implement extension of the current conventional approach. However, this approximation still would not account for the interactions of the different processes, something that can only be achieved in an integrated model. According to Statement 1, this approach is in particular not sufficient for surface loading.

Therefore, at least for the modeling of the geodetic signals of the fluid envelop, a dynamic Earth system model with coupled atmosphere, ocean and solid Earth modules needs to be developed in order to achieve a self-consistent modeling of most of these processes. However, the secular velocities are mainly due to plate tectonics, plate boundary deformation, and, in formerly glaciated areas, glacial isostatic adjustment. Accurate dynamic plate tectonic models predicting the plate motion and boundary deformation are not available and will not be in foreseeable future. Similarly, geophysical models for glacial isostatic adjustment show a wide range of predictions with no reference model emerging. At least for these processes, the DREM would have to include empirical models. The recent success with empirical models based on a combination of space-geodetic observations and geophysical models for the Eurasian and North American plates indicates that such models can be set up with high accuracy for individual plates. For the deformational zones, empirical models will be more demanding and require specific geophysical models. In particular in these areas, assimilation of high resolution observations from SAR and other imaging techniques will also have to be considered.

Also for the integrated model component addressing the interaction of the hydrological cycle with the solid Earth, the expected accuracy of a dynamic model is not sufficient, particularly for longer time scales. Therefore, this component of the DREM to some degree will have to assimilate not only meteorological and oceanographic observations but also observations from a global network of geodetic tracking stations, as well as observations of the gravity field and the Earth's rotation.

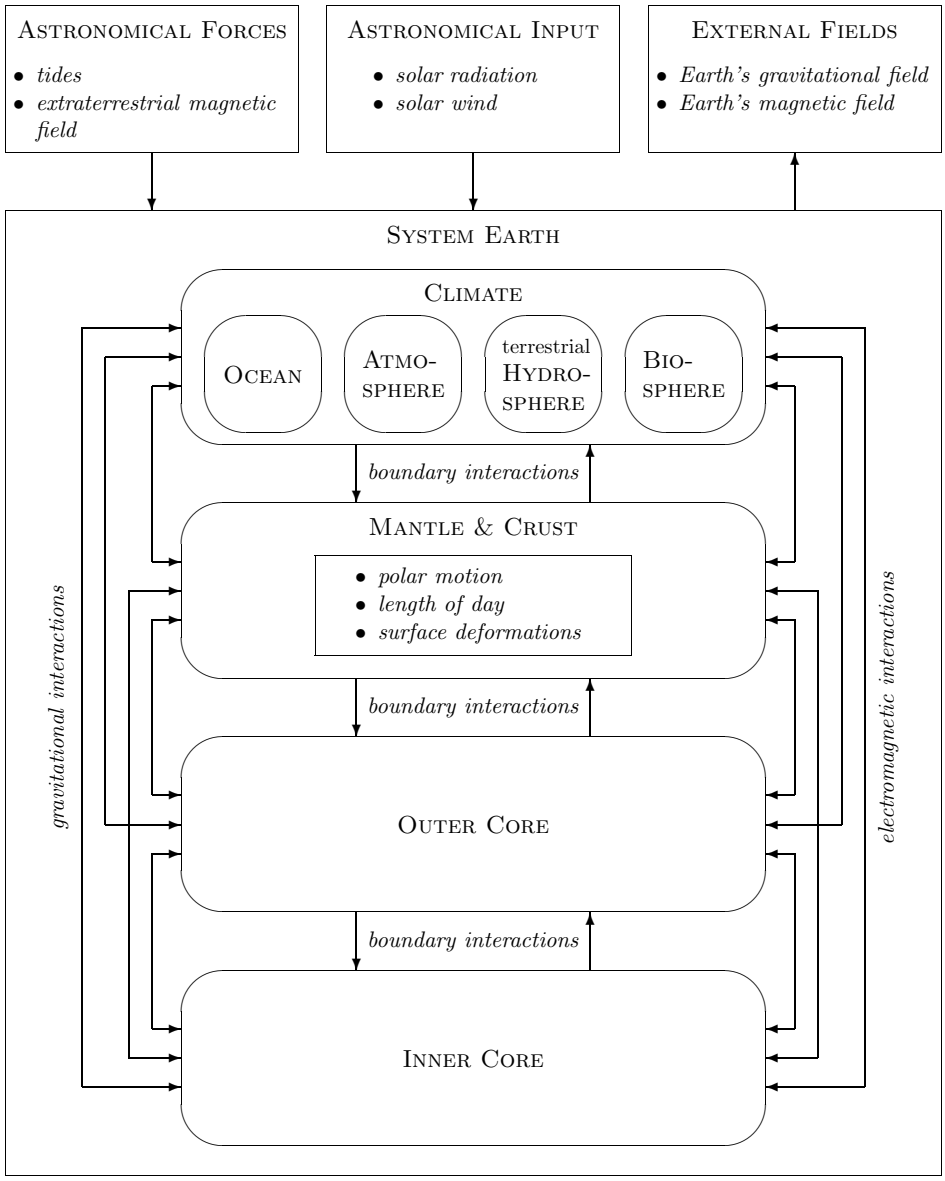

Figure 3. Components of the Earth system and their mechanical interactions. The Earth system can be viewed as composed of subsystems such as crust and mantle, outer and inner cores, and the fluid envelop of the solid Earth. The latter consists of ocean, atmosphere, and terrestrial hydrosphere, which are the prominent components of the climate system. We have chosen not to separate the cryosphere from the ocean and terrestrial hydrosphere but rather consider the ice load on land as part of the terrestrial hydrosphere and sea ice as part of the ocean. The biosphere is also interacting with the components of the climate system, and, considering the anthroposphere as part of the biosphere, also the solid Earth. The subsystems interact through surface forces at the joining boundaries and through volume forces (gravitational and electromagnetic). The overall system is subject to external forces including tidal forces and the extra-terrestrial magnetic field. From Plag (2006a).

Statement 5 (S5): *In order to capture geophysical signals unbiased and unmodified in space-geodetic time series of surface displacements, a reference frame approach based on a dynamic reference Earth model is required.*

5 Considerations concerning a DREM

(To a large extent, this Section is taken from Herring et al., 2007).

The Earth is a complex system composed of a number of dynamic subsystems that are characterized by different spatial and temporal scales and interacting with each other through surface and far-field forces. Internally, mass is rapidly redistributed in the fluid atmosphere and ocean, the global distribution of ice, snow, and water is continuously changing, the fluid core is undergoing some type of hydromagnetic motion, the mantle is both thermally convecting and rebounding from the glacial loading of the last ice age, and the tectonic plates exhibit slow motion as well as more rapid deformations in the boundary zones. Externally, forces due to the gravitational attraction of the Sun, Moon, and planets also act upon the Earth. The internal dynamical processes and external gravitational forces exert torques on the solid Earth and displace its mass, thereby causing the Earth's shape, gravity field, and rotation to change. The emerging properties and system behavior are sophisticated and models predicting the system state and trends have to

be inherently complex. Only if all these processes significant at the anticipated accuracy level can be modeled and predicted in a consistent Earth system model can we expect to make progress towards the proposed DREM.

For the modeling of the mechanical processes in the Earth system, the system can be viewed as composed of subsystems such as crust and mantle, outer and inner cores, and the fluid envelop of the solid Earth as sketeched in Figure 3. These subsystems interact through surface forces at the joining boundaries and through volume forces due to gravity or electromagnetic fields. In this mechanical view, the geometry, gravity field and rotation of the solid Earth are determined by the forces acting on the solid Earth, which include not only the external tidal forces but also the surface forces from surface loading, the volume forces due to changes in rotation and gravity field, as well as forces associated with convection or rapid redistributions of mass during earthquakes. In addition to the mechanical forces, on longer time scales we also have to consider thermo-dynamical forcing driving the convection in the Earth's mantle and core and creating phenomena such as volcanism and plate tectonics. However, for a description of the main characteristics of the geodetic variables, the mechanical view provides a valid basis.

Modeling of the mechanical behavior of the geosphere traditionally attempts to describe the whole Earth by a single system of equations specialized for specific phenomena (see e.g. Lambeck, 1988; Wahr, 1981, for rotation and loading deformations, respectively). In order to be feasible, this approach requires a high degree of simplification and many interactions and feedbacks have to be neglected. Consequently, even the most advanced geophysical models presently available are highly simplified and, moreover, specialized for the description of specific phenomena (such as nutation, Earth tides, surface deformations, geoid anomalies, glacial loading).

Over the last decades, several studies have demonstrated that complex systems can be modeled using a modular approach, with the individual modules representing subsystems or components that interacting through boundary conditions (surface forces, energy transfer, and particle transfer), and far-field interactions (gravimetric and electromagnetic volume forces). Complex climate models are built in this way, with separate submodules, for example, for the ocean, atmosphere, cryosphere, clouds, and land surface.

In a modular approach to the dynamics of a rotating planet, the planet is represented by a number of physically defined subsystems coupled to each other both by boundary conditions and far-field interactions. Thereby, different subsystems are described each on its own by dynamical equations. Couplings between different subsystems in this approach have to be defined independent of the structure and dynamics of the subsystems as physically meaningful quantities, for example, forces, moments or fields. There might be, moreover, external excitations acting on one or several particular subsystems such as for instance a tidal potential.

With respect to geodetic parameters, integrated systems have been studied mainly for Earth rotation. Jüttner & Plag (1999) used a simple modular model (*Dynamical Integrated Modular Earth Rotation System*, DIMERS), with submodels for the Earth's mantle, fluid core, and solid core, as well as the atmosphere and ocean to study system characteristics and to model polar motion forced by atmospheric loading. Based on a system model (*Dynamic Model for the Earth Rotation and Gravity*, DyMEG) similar to DIMERS, Seitz et al. (2005) studied the noise characteristics of polar motion, while Thomas et al. (2005) investigated the contribution of the ocean to polar motion excitation.

These model studies demonstrate that a modular approach to an Earth system model serving geodetic applications is feasible. In particular, these model studies show that so-called emerging system properties (e.g., the model periods of the Chandler wobble and nearly diurnal wobble) are sensitive to sub-model properties and coupling between the submodels, and these models allow the studying of the emerging properties as function of model parameters.

The modular approach allows for successive sophistications individually inside each of the subsystems without requiring any changes in the other subsystem. The only demands on the mathematical description of the dynamics of a subsystem are that it has to supply the other subsystems with time-dependent values of the prescribed physical coupling parameters and that it has to work with such coupling parameters supplied to it by other subsystems at each time-step anew. Of course, special attention has to be paid to the definition of the interactions right at the outset. Indeed, the isolation of subsystems of the planet and convention on the kind of their mutual interactions defines the structure of the modular theory. Unlike changes within any subsystem, the mere addition of a new interaction of two subsystems requires changing both of them. Moreover, the introduction of a new subsystem even requires changing all other subsystems interacting with the new one.

The choice of subsystems already characterizes a certain structure of the planetary interior and of the circumstances at the planet's surface. For the DREM, the appropriate choice of modules will be pivotal for the accuracy of

the model predictions. It can be expected that submodules will have to be introduced for different time scales. For example, the modeling of co- and postseismic processes may require a module separate from the one used for surface loading. In the end, the DREM may turn out to be a combination of a large number of models for various processes, which run in parallel and interact through boundary conditions and far-field forces, with the overall temporal model development "guided" by geodetic observations in real-time.

Model validation will be a key issue. The recent success of Gross et al. (2007b) in quantifying the level of consistency of surface mass estimates from geometric shape variation (GPS), gravity variations from space (GRACE), and Earth rotation (GPS and SLR). For most of the degree-2 terms, predictions of a multi-component model for surface mass are in reasonable agreement with all or most surface mass terms inverted from the observations of the different space-geodetic techniques. This indicates that these observations can be used in the validation of an integrated dynamic model. Other reference frame invariants like baseline lengths and angles between pairs of baselines could also support model validation. In fact, an integrated dynamic model ensuring consistency across all components of the hydrological cycle as well as across the three areas of geodesy would enable a validation with comparison of observed to predicted time series without the global spatial filtering inherent in the current approach.

6 Challenges to meet

With respect to a fully integrated model, Jüttner & Plag (1999) identified a number of challenges in developing a consistent theory for an advanced model with more realistic representation of all submodels. For most subsystems, individual reference frames will be needed, and in order to exchange body forces and boundary conditions between the system, the relation of the individual frames to a common model frame will have to be determined. For some of the submodels, such as the ocean circulation models, feedback from a deforming solid Earth with variable rotation is not sufficiently considered.

Challenges are also in the modeling of the solid Earth processes themself. Unlike a uniform description of the rotating planet as a whole, a modular theory of planetary dynamics requires direct time domain integration as an initial value problem for basically two reasons. First, the transformation into the frequency or Laplace domain and back into the time domain by a Greens function formalism requires linearity of the mathematical description of the whole system dynamics. That would restrict any subsystem model to a linear theory. The modular approach, however, should not restrict the internal structure of the subsystems in any way except for the match of couplings. Secondly, the definition of a boundary value problem refers to boundaries of particular subsystems but is characterized by eigenmodes of the system as a whole. Thereby additional links between all the distinct subsystems are introduced which are not physically determined as interactions of subsystems but mathematically as matches of certain kinematic patterns. In the treatment as boundary value problem a complete classification of possible types of normal or eigenmodes has to be achieved beforehand. This classification has to be done anew after any substantial change in any subsystem thus contradicting the spirit of the modular approach. Contrarily, in the modular approach to an initial value problem new properties of the whole system emerge in the course of integration.

For an initial approximation, some of the subsystems could be rather simple models. As explained above, in a modular DREM, the internal structure of the individual modules is not visible to the other modules. Interactions between modules are solely through surface and volume forces. Consequently, each module can be a complex model with full response to the forces exerted by the other modules or it can be represented through prescribed time series of the volume and surface forces associated with that module. For example, the atmosphere module could be a highly complex circulation model fully responding to the gravitational forces of all other modules, or it could provide the surface and volume forces as computed from the mass, pressure and wind fields of an independent meteorological models. Similarly, the ocean module could be a fully coupled ocean circulation model responding to ocean bottom displacements and Earth's rotation and gravity field changes, or it could provide the surface and volume forces as computed from the mass and current distribution of a decoupled model. For the terrestrial hydrosphere including the cryosphere, the situation is more complex, since mass changes normally imply exchange of mass with atmosphere and ocean, and conservation of mass across the global hydrological cycle is a key issue.

In an initial DREM, for the atmosphere and terrestrial hydrosphere, decoupled models could be chosen. For the ocean, a decoupled model would (in addition to the circulation changes) at least have to account for the surface

forcing from the atmosphere (pressure and wind forcing of a barotropic model) and the mass redistribution in the ocean caused by the gravity field changes and surface displacements (dynamic sea level equation). In all these cases, the pressure anomaly on the solid Earth's surface and the Newtonian gravity signal need to be calculated and provided to the other modules.

In the following, we will illustrate a few problems in providing these anomalies (surface pressure anomaly and Newtonian gravity signal) using the example of the atmosphere. These problems derive from differences in model orography and Earth topography, mass conservation, model resolution versus resolution required to get realistic anomalies, and decadal variations challenging the definition of a reference level against which the anomalies can be computed.

There are significant differences between the atmospheric model orography and the actual topography as deduced from ETOPO5. One reason for that is that the model orography is based on a spherical harmonic expansion, which smooths the orography considerably. Even more importantly, the orography in the meteorological models is not intended to match the topography accurately but rather the dynamical effects of the low-resolution orography should be a proxy for the expected dynamical effects of the topography. This results in regional large differences between model orography and Earth's topography. In Figure 4, we show the 2.5 degree land topography as derived from the ETOPO5 data together with the orography as implemented in the NCEP reanalysis model. The differences between the ETOPO5 topography and the model orography reach more than ± 2000 in mountainous regions. Although these differences are smaller for models with higher resolution, significant differences persist for all global models. Considering the exponential dependence of pressure on topographic height, surface pressure anomalies at model orography are significantly different from the anomalies at topographic height. This poses the problem that surface pressure anomalies need to be computed from meteorological model output at topographic height with high spatial resolution. Moreover, for the direct Newtonian gravity signal of the atmosphere, the actual topography needs to be taken into account.

The global mean of the differences (NCEP - ETOPO5) is 10.7 m. Thus, computing the air pressure at the Earth topography instead of model orography results in a change of the total mass of the atmosphere. This change could be absorbed by the mean pressure surface, which is used to compute the pressure anomaly. However, the change in total atmospheric mass is time variable, depending on how much mass is in orography areas below or above topography. This effect has not been assessed quantitatively but could potentially be significant, in particular for the Newtonian gravity signal.

An issue that results from the differences in Earth topography and model orography as well as the relatively low resolution of the meteorological models is the fact that the air pressure anomaly needs to be computed at topographic height. Since air pressure and pressure anomaly depend roughly exponentially on topographic height, the anomaly has to be given with high spatial resolution. Currently, it is not clear what spatial resolution is required in order to meet the accuracy goals of GGOS. However, based on the fact that most of the loading signal derives from the nearby pressure field, we can expect that a resolution of $<< 1^\circ$ will be necessary. Therefore, the spatial resolution of the meteorological dataset, which is 2.5° for the publically available datasets and 1.25° for the meteorological models, is not sufficient to represent the variations in topographic height and the effect on the air pressure anomaly in an appropriate way. Consequently, the pressure $p(x, h_\mathrm{t})$, where $x = (\lambda, \phi)$ is a point at the Earth's surface, and h_t is the topographic height of this point, has to be interpolated from the available datasets.

The meteorological datasets of NCEP/NCAR and ECMWF provide both pressure $p(x, 0)$ at *Mean Sea Level* (MSL) and the pressure $p(x, h_\mathrm{o})$ at the model orography with orographic height h_o. In addition, a number of other parameter are available at the model orography as well as at selected isobar levels. All datasets are available as spherical harmonic expansion and as grids, both with a spatial resolution of 2.5°.

In principle, there are several approaches to derive $p(x, h_\mathrm{t})$ with different characteristics in terms of accuracy, data requirements and computational load:

P1: The grided pressure and temperature at mean sea level are interpolated spatially and from these values, the pressure at topographic height is computed based on an approximate solution of the hydrostatic equation. Pressure and temperature at sea level show smooth spatial variations, so that the error due to spatial interpolation is small. This approach is associated with a low computational load, and data requirements are restricted to the pressure and temperature field at MSL. Accuracy is compromised since both air temperature and air pressure at

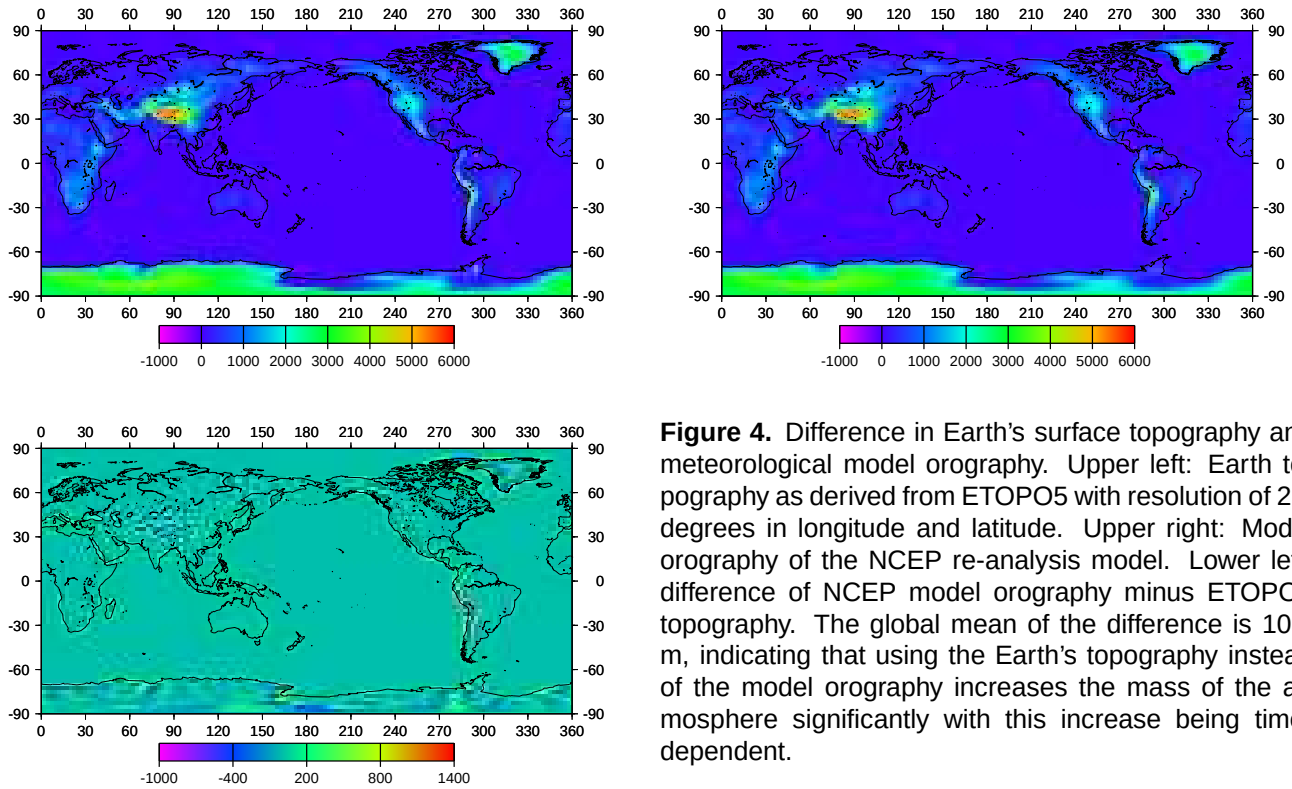

Figure 4. Difference in Earth's surface topography and meteorological model orography. Upper left: Earth topography as derived from ETOPO5 with resolution of 2.5 degrees in longitude and latitude. Upper right: Model orography of the NCEP re-analysis model. Lower left: difference of NCEP model orography minus ETOPO5 topography. The global mean of the difference is 10.7 m, indicating that using the Earth's topography instead of the model orography increases the mass of the atmosphere significantly with this increase being time-dependent.

MSL are not modeled parameters but rather extrapolated from the respective fields at orographic height, with in particular the air pressure extrapolation being inaccurate.

P2: The spherical harmonic expansions of pressure and temperature at the model orography are evaluated with the required spatial resolution and then propagated from h_{o} at the interpolated point (which can be calculated from the spherical harmonic expansion of the model orography) to h_{t}. Computational load is high (many evaluations of the spherical harmonic expansions), while data requirements are the pressure and temperature fields at orographic heights. In addition, a spatially dense grid of the orographic heights needs to be computed once in order to avoid evaluation of the spherical harmonic expansion of the model orography for each time sample. For most points on land, the difference $\delta_h = h_{\mathrm{t}} - h_{\mathrm{o}}$ will be much smaller that h_{t}, and the accuracy of this approach can be expected to be high. In addition, all required fields are modeled quantities and internally consistent.

P3: The geopotential, which is given for a number of isobars, is used to determine the height of these isobars and from these $(p(x), h(x))$ samples, $p(x, h_{\mathrm{t}})$, is interpolated. This approach requires the geopotential field for up to ten isobars and two interpolations (first to the spatial point and then in height). The computational load is comparable to P1, and the accuracy depends on the accuracy of the interpolation algorithm for the geopotential heights.

In Appendix A, we assess the accuracy of the three algorithms based on unpublished work by one of us (Plag). As a result, it is found that P1 is of unaccceptable accuracy mainly due to the fact that the required parameters are not model parameters. They are extrapolated from the model orography with an approximation algorithm (White, 2003) leading to considerable errors particularly over the large ice sheets and high mountain areas.

Statement 6 (S6): *Air pressure at topographic height cannot be computed from predicted air pressure at mean sea level due to large errors of this quantity. Instead, air pressure at topographic height has to be computed from air pressure at model orography or interpolated from the geopotential heights of isobars with the former being more accurate.*

The reference surface for air pressure, which is used to computed the pressure anomaly needs to be chosen carefully in order to avoid a permanent deformation of the reference frame (comparable to degree-0 tidal terms). The reference surface is likely to be model dependent, and thus will be different, for example, for NCEP and ECMWF data, as well as for reanalysis and operational data. But we can also expect temporal variations in the mean pressure of an interval of, for example, ten years. In Appendix B, we show the variations of the decadal pressure at topographic height for the ERA40 reanalysis dataset. Large interdecadal variations are found in a latitude-band around Antarctica, reaching nearly -6 HPa over the 40 year-interval, while in other areas values up to +3 HPa occur. While it is not clear to which extent these trends are model artifacts, these large interdecadal variations potentially introduce secular trend particularly in height.

These interdecadal variations also require careful considerations in the choice of a conventional reference surface for air pressure at topographic height. The choice of the time interval used to compute the reference surface is important as it determines what trends and decadal variations we introduce into any loading prediction. Considering that the reanalysis and operational products provided by NCEP and ECMWF use significantly different model orographies with different temporal evolution, thus requiring different pressure reference surfaces, which one may want to choose in a way that the differences in the anomalies computed from the products of the two centers are as small as possible, thus avoiding the need to choose one over the other.

Statement 7 (S7): *Interdecadal variation in predicted air pressure at topographic height are found to be of an order significant at the accuracy level of* 10^{-9} *and thus require a careful choice of the conventional reference pressure fields. Moreover, intermodel differences necessitate model-specific reference pressure fields.*

It is mentioned here that similar considerations also apply to air temperature and to any other meteorological parameter taken from observations or models that influence the final solution of geodetic analysis. In all these cases, choosing a reference surface which leads to an anomaly with non-zero mean may (and in the case of loading does) introduce a permanent deformation of the solid model Earth, and thus the reference polyhedron (or in the future a DREM), if the anomalies enter the geodetic analysis or the predicted displacements and gravity variations are taken into account in the geodetic analysis. Thus, the goal could be to choose the reference surfaces in such a way that the computed anomalies have a (space-dependent) mean (over time) as close to zero as possible.

It is also noted that a similar situation applies to ocean models, where the reference ocean bottom pressure field depends on time interval and model, and to terrestrial hydrological models, where the reference water column/surface pressure also depends on model and time interval. For all these contributions, (conventional) reference pressure fields need to be chosen carefully in order to avoid permanent deformations of the reference frame.

As long as an integrated model of the global hydrological cycle is not available that could be used to determine the surface load anomaly, air pressure, ocean pottom pressure and terrestrial water storage need to be extracted from individual models. For each component, several models exists with the predicted surface anomalies differing significantly. Therefore, the question arises whether it would be more appropriate to choose for the Conventions one model over the others, or to use an (weighted) average/combination of the surface anomalies determined from a conventional suit of models. An informed decision would require more studies of the actual differences at topographic height (also for the ocean bottom), and a comparison of the average anomaly to the individual sample anomalies.

A critical issue are model inconsistencies in terms of orography, physical assumptions, and available parameters, that can complicate the combination of models. Moreover, model improvements will be model-specific in terms of what is improved and when. Therefore, a careful monitoring of the model history and model output will be required.

For air pressure, the response of the ocean to mechanical forcing (pressure and wind) is another issue which is currently still undecided. The two widely used approximation of "no response" (NIB) and "inverted barometer" (IB) response are know to be inaccurate, with the uncertainties depending on the time scale of the air pressure variations. Moreover, any wind effect is not accounted for. Plag (2006b) showed that regional interdecadal variations in air pressure introduced significant variations in mean sea level, which compensate largely but not completely for these long-period atmospheric circulation changes, while over land, these are fully preserved. However, for shorter time scales of weeks and below, the NIB is increasingly inaccurate, depending on the geographical setting. Therefore, a more advanced approach is required in order to meet the accuracy goal of GGOS.

Statement 8 (S8): *For the computation of the global surface pressure anomaly, the response of the ocean to mechanical atmospheric forcing (pressure and wind) has to be modeled with a global hydrodynamical (barotropic) model.*

We have not addressed the loading calculation itself. Van Dam et al. (2003) discussed the effect of Earth model and numerical algorithms in detail and showed that the associated uncertainties are smaller than those resulting from the load anomaly itself. However, once the computation of the load anomalies have been improved, the uncertainties due to loading computations should be reassessed.

Most of what has been stated so far applies in general to the definition of the temporal evolution of the reference polyhedron, i.e., the extension of eq. 1. A remaining (and long-standing) question is which loads have subdiurnal or sub-weekly variations large enough to require the inclusion in the station motion model for daily or weekly analyses, i.e. which of these processes need to be accounted for in eq. 2 or eq. 3. It is expected that ocean bottom pressure variations are slow and thus not relevant for analyses with daily or weekly intervals. For the terrestrial hydrosphere, most loading variations also exhibit longer time scales, with the exception of large flooding events, where subweekly changes can be significant. However, for air pressure, sub-daily and sub-weekly variations are large, particularly at higher latitudes. In Appendix C, we consider the statistics of daily and weekly air pressure changes. Maximum daily and weekly ranges reach up to 60 HPa and 90 HPa, respectively, with the largest variations found around Antarctica, over the North Atlantic and the North Pacific and adjacent land areas. Over the ocean, these large variations will be partly compensated by the ocean's response to the atmospheric forcing. Mean daily and weekly air pressure changes reach 10 HPa and 40 HPa, respectively. The quantitative estimates indicate that at least in high-latitude areas, air pressure loading can induce significant changes in the station position over the analysis interval, and including the predicted displacements in the station motion model could improve the analysis results.

Statement 9 (S9): *The displacements induced by the atmospheric loading at high latitudes exhibts significant sub-daily and sub-weekly variations.*

7 Immediate improvements

While it is clear that the development of a fully consistent and integrated DREM will take time and require the effort of many, there are a number of steps that could lead to immediate improvements. In particular, we consider the following steps as reachable in relatively short time:

I1: By extending the definition of the "regularized coordinates" (eq. 1) to a model including predicted non-linear motion (eq. 3, with not only surface loading, but also displacement field of large earthquakes accounted for), the effect of the global filtering inherent in the current definition could be significantly reduced.

I2: Operational prediction of displacements due to atmospheric loading should be improved through (1) better modeling of the ocean's response to atmospheric forcing (hydrodynamical barotropic model); (2) a conventional

approach to the (model-dependent) reference surface(s) for air pressure; and (3) a conventional approach to the handling of inter-model differences.

I3: Setting up of an operational computation of ocean-bottom pressure anomalies (either model- or GRACE-based) and the computation of the induced surface displacements in support of I1.

I4: Setting up of an operational computation of terrestrial water storage anomalies (either model- or GRACE-based or a combination) and the computation of the induced surface displacements in support of I1.

I5: A consistency check based on mass conservation should be used to link the anomalies of I2 to I4 together, and to ensure that large errors in mass conservation (which would introduce biases in the total displacements) are detected/avoided.

8 Recommendations

Recommendation 1:
Recognizing that
atmospheric loading is a geophysical process inducing surface displacements at sub-daily to interannual time scales significant at an accuracy level of 10^{-9} and that
signals of atmospheric loading in the shape, gravity field and rotation of the Earth can be predicted with high accuracy
it is recommended that
as a first step a dynamic reference model is developed and validated that consistently predicts with low latency the atmospheric loading signal in the surface displacement, gravity field and rotation of the Earth and that
these predictions are taken into account in the determination of the ITRF as well as the products providing low-latency access to ITRF.

Recommendation 2:
Recognizing that
mass redistribution in atmosphere, oceans, and terrestrial hydrosphere are inherently related through processes in the global hydrological cycle and that
these mass redistributions cause surface displacements at sub-daily to interannual time scales significant at an accuracy level of 10^{-9} and that
the feedback between the individual components (reservoirs) of the hydrological cycle as well as the solid Earth also cause significant signals in the shape, gravity field and rotation of the Earth
it is recommended that
a dynamic Earth model is developed and validated that consistently predicts the geodetic signals of mass redistribution in the global hydrological cycle and that
accounts for the geophysical interactions between the reservoirs of the hydrological cycle and the solid Earth.

Recommendation 3:
Recognizing that
monitoring of point motion and detection of "anomalous motion" are key application of a modern global reference frame and space geodetic techniques, and that
for many applications a predictive reference frame is required, and that
such a reference frame needs to be based on a Dynamic Reference Earth Model (DREM)
it is recommended that
a DREM is developed that accounts for all know geophysical processes significant at the level of 10^{-9} and that predicts consistently the signals in Earth shape, rotation and gravity field caused by these processes.

References

Altamimi, Z. & Boucher, C., 2002. The ITRS and ETRS89 relationship: new results from ITRF2000, in *EUREF Publication No. 10*, edited by J. A. Torres & H. Hornik, no. 23 in Mitteilungen des Bundesamtes für Kartografie und Geodäsie, pp. 49–52, Verlag des Bundesamtes für Kartographie und Geodäsie, Frankfurt am Main.

Blewitt, G., 2003. Self-consistency in reference frames, geocenter definition, and surface loading of the solid earth, *J. Geophys. Res.*, **108**, 10.1029/2002JB002082.

Blewitt, G. & Clarke, P., 2003. Inversion of earth's changing shape to weigh sea level in static equilibrium with surface mass redistribution, *J. Geophys. Res.*, **107**, DOI: 10.1029/2002JB002290.

Blewitt, G., Lavallée, D., Clarke, P., & Nurutdinov, K., 2001. A new global mode of earth deformation: Seasonal cycle detected, *Science*, **294**, 2342–2345.

Blewitt, G., Bennett, R., Calais, E., Herring, T., Larson, K., Miller, M., Sella, G., Snay, R., & Tamisiea, M., 2004. First report of the Stable North America Reference Frame (SNARF) Working Group, *Eos, Trans. Am. Geophys. Union*, **85**(17), Jt. Assem. Suppl., Abstract G21C–01.

Clarke, P. J., Lavallée, D. A., Blewitt, G., van Dam, T., & Wahr, J. M., 2005. Effect of gravitational consistency and mass conservation on seasonal surface mass loading models, *Geophys. Res. Lett.*, **32**, doi: 10.1029/2005GL022441.

Dong, D., Fang, P., Bock, Y., Cheng, M. K., & Miyazaki, S., 2002. Anatomy of apparent seasonal variations from GPS-derived site position time series, *J. Geophys. Res.*, **107**, 2075, doi:10.1029/2001JB000573.

Dziewonski, A. M. & Anderson, D. L., 1981. Preliminary reference Earth model, *Phys. Earth Planet. Int.*, **25**, 297–356.

Farrell, W. E., 1972. Deformation of the Earth by surface loads., *Rev. Geophys. Space Phys.*, **10**, 761–797.

Gross, R., Beutler, G., & Plag, H.-P., 2007. Integrated scientific and societal user requirements and functional specifications for the ggos, in *The Global Geodetic Observing System: Meeting the Requirements of a Global Society on a Changing Planet in 2020 – The Reference Document*, edited by H.-P. Plag & M. Pearlman, Global Geodetic Observing System, available at http://geodesy.unr.edu/ggos/ggos2020/.

Gross, R. S., Lavalle, D. A., Blewitt, G., & Clarke, P. J., 2007. Consistency of Earth rotation, gravity, and shape measurements, vol. 131 of **International Association of Geodesy Symposia**, Springer Verlag, Berlin, in press.

Herring, T. A., Altamimi, Z., Plag, H.-P., Poli, P., & Ray, J., 2007. The future geodetic reference frame, in *The Global Geodetic Observing System: Meeting the Requirements of a Global Society on a Changing Planet in 2020 – The Reference Document*, edited by H.-P. Plag & M. Pearlman, Global Geodetic Observing System, available at http://geodesy.unr.edu/ggos/ggos2020/.

Jüttner, H.-U. & Plag, H.-P., 1999. On modelling of earth rotation variations in an integrated model and appropriate frame of reference, in *3. DFG Rundgespräch zum Thema Bezugssysteme*, edited by M. Schneider, vol. 5 of **Mitteilungen des Bundesamtes für Kartographie und Geodäsie**, pp. 59–62, Bundesamtes für Kartographie und Geodäsie.

Kierulf, H. P., Plag, H. P., Bingley, R. M., Teferle, N., Demir, C., Cingoz, A., Yildiz, H., Garate, J., Davila, J. M., Silva, C. G., Zdunek, R., Jaworski, L., Martinez-Benjamin, J. J., Orus, P., & Aragon, A., 2007. Comparison of GPS analysis strategies for high-accuracy vertical land motion, *Phys. Chem. Earth*, p. in press.

Lambeck, K., 1988. *Geophysical Geodesy - The Slow Deformations of the Earth*, Oxford Science Publications.

Lavallee, D. & Blewitt, G., 2002. Degree-one Earth deformation from very long baseline interferometry, *Geophys. Res. Lett.*, **29**(20), doi:10.1029/2002GL015883.

Lavallée, D., van Dam, T., Blewitt, G., & Clarke, P., 2006. Geocenter motions from GPS: A unified observation model, *J. Geophys. Res.*, In press.

McCarthy, D. D. & Petit, G., 2004. *IERS Conventions 2003*, IERS Technical Note 32, International Earth Rotation Service, Also available at http://www.iers.org.

Plag, H.-P., 2006. National geodetic infrastructure: current status and future requirements - the example of norway, Bulletin 112, Nevada Bureau of Mines and Geology, University of Nevada, Reno, 97 pages.

Plag, H.-P., 2006. Estimating recent global sea level changes, in *Dynamic Planet – Monitoring and Understanding a Dynamic Planet with Geodetic and Oceanographic Tools*, edited by P. Tregoning & C. Rizos, vol. 130 of **International Association of Geodesy Symposia**, pp. 39–46, Springer Verlag, Berlin.

Plag, H.-P., Nørbech, T., & Kristiansen, O., 2002. Effects of intraplate deformations on fixing regional reference frames, in *EUREF Publication No. 10*, edited by J. A. Torres & H. Hornik, vol. 23 of **Mitteilungen des Bundesamtes für Kartografie und Geodäsie**, pp. 118–124, Verlag des Bundesamtes für Kartographie und Geodäsie, Frankfurt am Main.

Ray, J., Altamimi, Z., van Dam, T., & Herring, T., 2007. Principles for conventional contributions to modeled station displacements, Position paper presented at the IERS Workshop on Conventions, Paris, September 22-23, 2007; available at http://www.bipm.org/utils/en/events/iers/Conv_PP1.txt.

Seitz, F., Stuck, J., & Thomas, M., 2005. White noise Chandler wobble excitation, in *Forcing of polar motion in the Chandler frequency band: A contribution to understanding interannual climate variations*, edited by H.-P. Plag, B. Chao, R. Gross, & T. van Dam, vol. 24, p. This issue, Cahiers du Centre Européen de Géodynamic et de Séismologie.

Thomas, M., Dobslaw, H., Stuck, J., & Seitz, F., 2005. The ocean's contribution to polar motion excitation - as many solutions as numerical models?, in *Forcing of polar motion in the Chandler frequency band: A contribution to understanding interannual climate variations*, edited by H.-P. Plag, B. Chao, R. Gross, & T. van Dam, vol. 24, p. This issue, Cahiers du Centre Européen de Géodynamic et de Séismologie.

Tregoning, P. & Herring, T. A., 2006. Impact of a priori zenith hydrostatic delay errors on GPS estimates of station heights and zenith total delays, *Geophys. Res. Lett.*, **33**, 1.23303 dio 10.1029/2006GL027706.

Van Dam, T., Plag, H.-P., Francis, O., & Gegout, P., 2003. GGFC Special Bureau for Loading: current status and plans, in *Proceedings of the IERS Global Geophysical Fluid Center Workshop, Munich, November 20-21, 2002*, edited by B. Richter, W. Schwegman, & R. Dick, no. 30 in International Earth Rotation and Reference System Service, IERS Technical Note, pp. 180–198.

Wahr, J. M., 1981. A normal mode expansion for the forced response of a rotating earth, *Geophys. J. R. Astron. Soc.*, **64**, 651–675.

Wdowinski, S., Bock, Y., Zhang, J., & Fang, P., 1997. Southern California Permanent GPS geodetic array: spatial filtering of daily positions for estimating cosesimic and postseismic displacements induced by the 1992 Landers earthquake, *J. Geophys. Res.*, **102**, 18,057–18,070.

Wdowinski, S., Bock, Y., Baer, G., Prawirodirdjo, L., Bechor, N., Naaman, S., Knafo, R., Forrai, Y., & Melzer, Y., 2004. GPS measurements of current crustal movements along the Dead Sea Fault, *J. Geophys. Res.*, **109**, (B05403), 1–16.

White, P. W. e., 2003. IFS Documentation Part IV: Technical and Computational Procedure (CY23R4), Tech. rep., European Center for Medium Range Weather Forecast.

A Computation of air pressure at topographic height

As stated in Section 6, we consider three algorithms (denoted as P1, P2, and P3, reaspectively) for the computation of air pressure at topographic height, with all three algorithms requiring additional modeled parameters.

In the following, we will assess the accuracy and computational requirements of the three algorithms based on unpublished work by one of us (Plag). For P1 and P2, propagation of pressure from h_1 to h_2 is required. In principle, this conversion can be done using the hydrostatic equation

$$\mathrm{d}p = -g(h)\rho(h)\mathrm{d}h \tag{6}$$

where g is the gravitational acceleration, and ρ the density. The height dependency of g can be neglected. ρ is given by the ideal gas equation

$$\rho(h) = \frac{p(h)}{RT_{\mathrm{v}}(h)}. \tag{7}$$

Here, $T_{\mathrm{v}}(h)$ is the virtual air temperature as function of height and R is the gas constant for air, which for normal air is

$$R = 2.8705 \cdot 10^6 \ \mathrm{cm^2 s^{-2} K^{-1}}. \tag{8}$$

The virtual air temperature is the temperature that dry air would have to have under the same pressure in order to have the same density as humid air with specific humidity s. The relation between the actual temperature T and the virtual temperature is

$$T_{\mathrm{v}} = T(1 + 0.608s), \tag{9}$$

where s is defined by the ratio of the density of the water vapour ρ_w to the density of the humid air. Thus,

$$s = \frac{\rho_w}{\rho_a + \rho_w}, \tag{10}$$

where ρ_a is the density of the dry air.

Combining equations (6) and (7) results into

$$\frac{\mathrm{d}p}{p} = -\frac{g\mathrm{d}h}{R \cdot T_{\mathrm{v}}} \tag{11}$$

In order to find an approximate solution to eq. (11), we assume isothermal layers. Integrating eq. (11) under this assumption for a layer between h_i and h_{i+1} and assuming a virtual temperature $T_{\mathrm{v}}(h) = T_{\mathrm{v}i}$ leads to

$$\ln p_{i+1} - \ln p_i = -\frac{g \cdot (h_{i+1} - h_i)}{R \cdot T_{\mathrm{v}i}} \tag{12}$$

which results into

$$p_{i+1} = p_i \cdot e^{-\frac{g \cdot (h_{i+1} - h_i)}{R \cdot T_{\mathrm{v}i}}}. \tag{13}$$

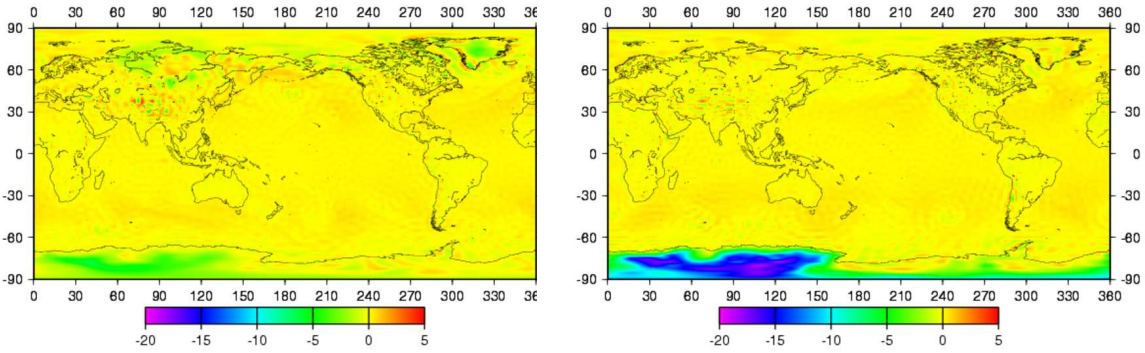

Figure 5. Differences δ^{geop} of air pressure at MSL. The quantity show is δ^{geop} as defined by eq. (16). Plots are for 2000/01/01/00 (left) and 2000/08/01/12 (right). Resolution of the datasets is 5 minutes. The scale is in HPa.

We denote the pressure computed using eq. (13) under the assumption that $T_{\mathrm{v}i} \approx T_{\mathrm{std}}(h_i) = T_0 - 0.006h_i$ as p^{isot}. This isothermal-layer approach represents a good approximation to the hydrostatic equation. For layer thickness of the order of ten meters, the error due to the isothermal-layer assumption is of the order of 10^{-4} for heights of up to 5000 meters.

However, the main errors of this approximation are due to (1) deviations of $T(h)$ from the standard approximation $T_{\mathrm{std}}(h) = T_0 - 0.006h$, and (2) deviations of T_{v} from T. P1 requires extrapolation over heights of more than 5000 m, while for P2, extrapolations are normally of the order of a few hundred meters and at maximum of the order of $\pm 10^3$ m (see above). Using T_{v} instead of $T_{\mathrm{std}}(h)$ the latter, would require to get the vertical profiles of model temperature and model humidity in order to compute the surface pressure anomalies.

For P3, we derive $p(x, h_{\mathrm{t}})$ from the geopotential heights of isobars. The meteorological datasets include the topography of surfaces of constant pressure given in geopotential meter, i.e., the geopotential heights Φ_i for a set of fixed pressure values $p_i,\ i = 1, ..., n$. The relation between the geopotential heights Φ and the topocentric heights h is simply

$$h(x) = \frac{\Phi(x)}{g(x)} \tag{14}$$

Since over small height differences, pressure is close to a exponential function, we have

$$\ln(p^{\mathrm{geop}}(h)) = \ln(p_i) + \frac{\ln(p_{i+1}) - \ln(p_i)}{h_{i+1} - h_i} \cdot (h - h_i). \tag{15}$$

This provides the means to determine the pressure at topographic height directly from the model output of geopotential heights of the different pressure levels.

According to ECMWF experts (Mariano Hortal, 2006, personal communication), P2 will give the most accurate results, while P3 is considered to be a reasonable approximation. In the following we compare the approaches P1 to P3 with each other, in order to assess the quality of P1. As a first test, we compare pressure p at MSL as provided by the ERA40 data to the pressure p^{geop} at MSL as derived from the geopotential heights using eq. (15) for the interpolation to zero height. Thus, we consider the differences

$$\delta^{\mathrm{geop}} = p^{\mathrm{geop}}(0) - p(0) \tag{16}$$

In Figure 5, we show these differences for two different days in winter and summer.

As expected, over the oceans the differences are within ± 0.5 HPa. Also, for most land areas, differences are below ± 1 HPa. Only for the large ice sheets and the Himalaya region, larger differences are found.

In order to assess these differences, we have computed statistical parameters of the differences for the full ERA 40 dataset. The mean value of δ^{geop} shows the same spatial pattern (Figure 6) as was already visible in the individual examples in Figure 5, i.e. values close to zero for most of the Earth's surface, with negative deviations over most of central Antarctica and Greenland, with maximum deviations below -10 HPa. The standard deviation over this

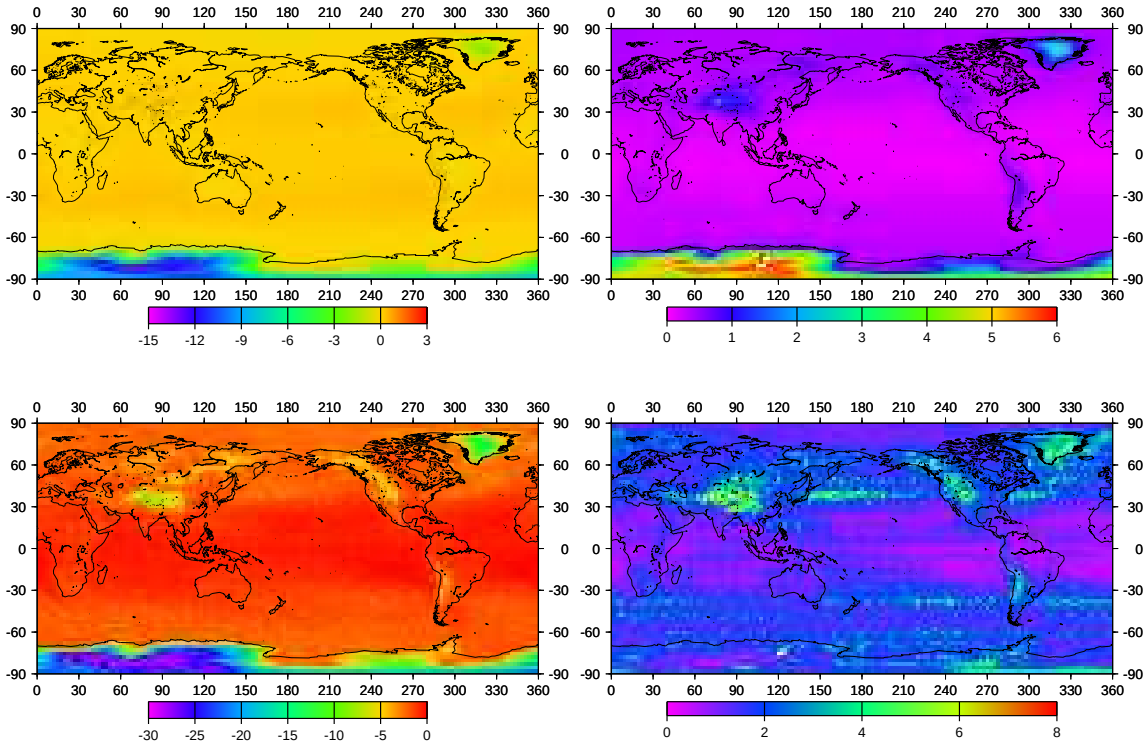

Figure 6. Statistics of differences δ^{geop} at MSL. The statistical parameters are mean (upper left), standard deviation with respect to mean (upper right), minimum (lower left), and maximum (lower right) of δ^{geop}. The parameters are computed for the six hourly samples in the interval 1958/01/01 to 2001/12/31.

mean reflects this pattern, but also shows increased values over most of the mountainous land areas. The minimum of δ^{geop} over the total ERA 40 time window reaches values close to -30 HPa over East Antarctica, while the maximum reaches values of up to 8 HPa over central Asia.

Considering the statistics of the daily and weekly ranges of δ^{geop} (Figure 7), we note that mean daily ranges are very small (< 2.5 HPa), while mean weekly ranges reach up to 7 HPa. Thus, most of the variability in δ^{geop} appears to be on interdiurnal time scales. However, the maximum daily ranges can reach more than 15 HPa in Antarctica, while maximum weekly ranges rarely exceed 20 HPa.

In summary, the detected differences between p^{geop} and the air pressure at MSL as provided by ERA 40 underline the inconsistencies between these two parameters. It is interesting to note that the spatial pattern in δ^{geop} seems to link the main problems to the central part of the large ice sheets, where $p^{\mathrm{geop}}(0)$ appears to be smaller than $p(0)$, while some problems also seem to exist over other mountainuous areas, though there $p^{\mathrm{geop}}(0)$ has a tendency to be larger than $p(0)$. The temporal characteristics of the differences seem to indicate that the variations in the differences are related to weather variability, with typical time scales of several days.

These large differences between $p(0)$ and $p^{\mathrm{geop}}(0)$ over land areas are due to the fact that $p(0)$ is derived from the surface pressure with an approximate algorithm, which does not lead to accurate MSL pressure values under the large ice sheets and the high mountain areas (White, 2003). These large difference rule out P1 as an approach to deduce accurate pressure values at topographic heights.

B Air pressure reference surfaces

The correct choice of the reference pressure is of considerable importance with respect to the geodetic reference frame. Any bias in the reference pressure will introduce a permanent load and deformation, and thus affect the reference frame. Therefore, here we study the stability of the mean pressure. For that, we computed the mean pressure at

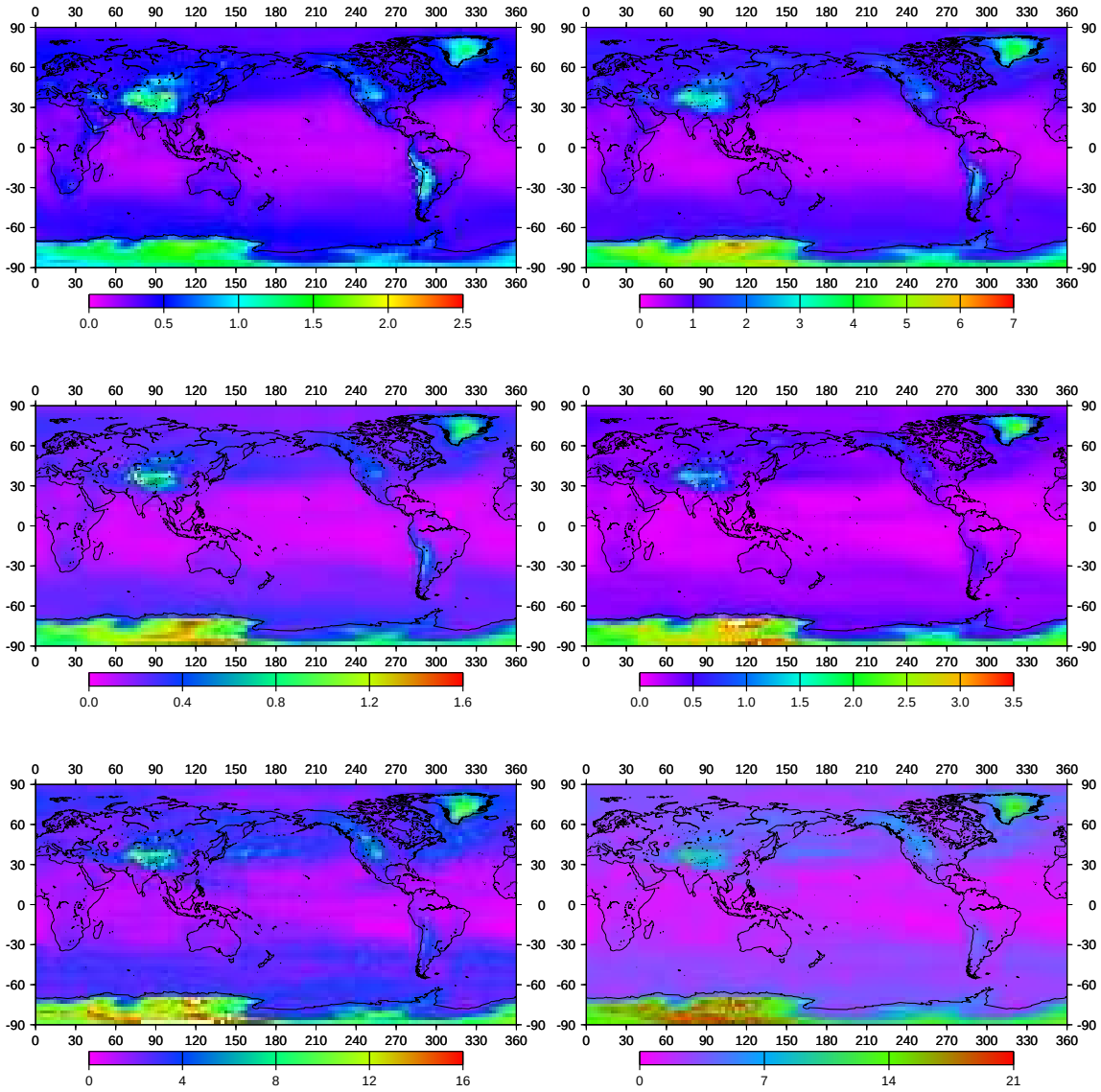

Figure 7. Daily and weekly ranges in the differences δ^{geop} at MSL. The quantities considered are the daily (left) and weekly (right) ranges of δ^{geop} as derived from the four samples in each day. The statistical parameters are the mean (top), standard deviation with respect to mean (middle), and maximum range (bottom). The parameters are computed for the interval 1958/01/01 to 2001/12/31. Spatial resolution of the datasets is 2.5 degrees.

topographic height for the complete ERA 40 window as well as for subsequent 10-year intervals.

Figure 8 shows the ten-year mean pressure for the interval 1992.0 to 2002.0 together with the differences between this surface and the previous three corresponding ten-year intervals. The differences are largest in a latitude-band around Antarctica, reaching nearly -6 HPa while in other areas values up to +3 HPa occur. These large inter-decadal variations introduce secular trend particularly in height. They also require careful considerations in the choice of a conventional reference surface for air pressure at topographic height.

C Statistics of air pressure at topographic height

In order to decide whether load-induced displacements should be taken into account in the station motion model of a geodetic analysis using a certain sample window (e.g., one day) or in the post-analysis reference frame alignment, the temporal variability of the displacements at sub-sample time scales is of importance. A simple characterization of

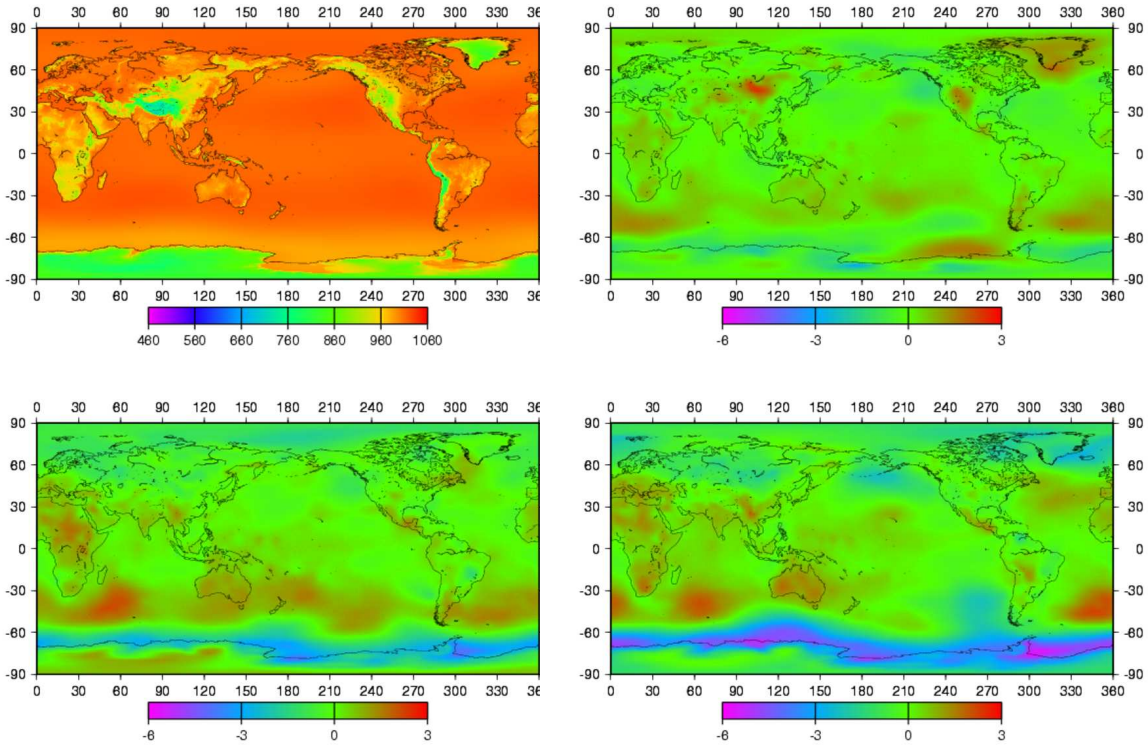

Figure 8. Mean decadal air pressure at topographic height. Quantity is the mean air pressure at topographic height computed with the isothermal layer approximation for a 10-year time interval. The diagrams show the mean for the time window starting at 1992 (top left), difference between this mean and the mean for the window starting at 1982 (top right), 1972 (bottom left), and 1962 (bottom right). Spatial resolution is 5 minutes. The scales are in HPa.

this variability is achieved by determining the range of air pressure anomalies over the sample window. However, the maximum and mean range over the sample window does not necessarily give the full picture.

For a given location, for each sample window, we will determine the pressure range. The distribution of these ranges over the total time interval considered will be characterized by the mean range $\bar{r}$, the maximum range $r_{\max}$, the variance over the mean ν_r, and the standard deviation σ_r.

The scanning of the era40 dataset with the resolution of the earth topography is extremely time-demanding, while the storage of the six-hourly surface pressure anomalies for a post-processing to compute the statistics is forbidding in storage demands. Therefore, the relations for all statistical quantities have to be written so that all quantities can be computed in one run together with the actual computation of the surface pressure anomalies.

This results in the following set of relations

$$\bar{r} = \frac{1}{N}\sum_{j=1}^{N} r_j \tag{17}$$

$$\nu_r = \frac{1}{N-1}\left(\sum_{j=1}^{N} r_j^2 - 2\bar{r}\sum_{j=1}^{N} r_j + N\bar{r}^2\right) \tag{18}$$

$$\sigma_r = \sqrt{\nu_r} \tag{19}$$

$$\tag{20}$$

In Figure 9, the statistics of daily and weekly air pressure changes at topographic height as deduced from the geopotential (approach P2, see Appendix A) are shown for the full ERA40 dataset. All statistical parameters (mean range, standard deviation over mean, maximum range) show a pronounced dependence on latitude, with the largest variations found for latitudes above 30°, while for low latitudes, all variations are generally very small. In the high latitude bands, maximum daily and weekly ranges reach up to 60 HPa and 90 HPa, respectively, with the largest variations found in a borad band around Antarctica, over the North Atlantic, the North Pacific and land areas adjacent to these water bodies. Over the ocean, these large variations will be partly compensated by the ocean's response to the atmospheric forcing, while over land, they are fully preserved. Mean daily and weekly air pressure changes reach 10 HPa and 40 HPa, respectively. As expected from the exponential dependence of air pressure on height, over areas with high topography, the ranges are generally smaller than over low-lying areas.

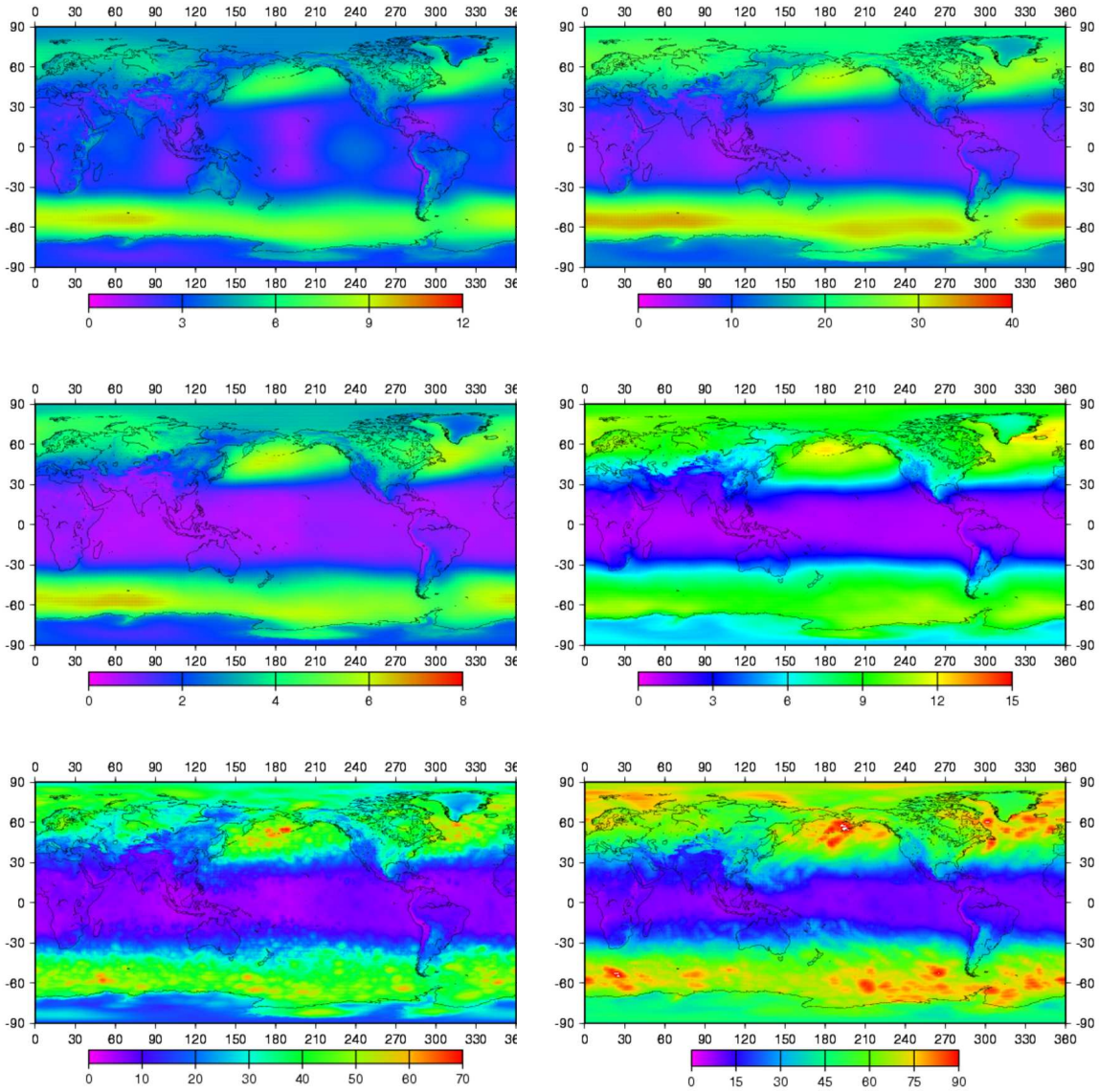

Figure 9. Daily and weekly ranges in air pressure at topographic height. The quantities considered are the daily (left) and weekly (right) ranges of $p(x, h)$ as derived from the four samples in each day. The statistical parameters are the mean (top), standard deviation with respect to mean (middle), and maximum range (bottom). The parameters are computed for the interval 1958/01/01 to 2001/12/31. Spatial resolution of the meteorological datasets is 2.5°, while the topography has a resolution of 5 minutes.